



**HAL**  
open science

## Supercritical millifluidic reactor for the synthesis of efficient GaN nanophotocatalysts

Prasaanth Ravi Anusuyadevi, Zachary S. Campbell, Arnaud Erriguible, Samuel Marre, Cyril Aymonier

► **To cite this version:**

Prasaanth Ravi Anusuyadevi, Zachary S. Campbell, Arnaud Erriguible, Samuel Marre, Cyril Aymonier. Supercritical millifluidic reactor for the synthesis of efficient GaN nanophotocatalysts. *Chemical Engineering Journal Advances*, 2023, 14, 100483 (9 p.). 10.1016/j.cej.2023.100483. hal-04053896

**HAL Id: hal-04053896**

**<https://hal.science/hal-04053896>**

Submitted on 31 Mar 2023

**HAL** is a multi-disciplinary open access archive for the deposit and dissemination of scientific research documents, whether they are published or not. The documents may come from teaching and research institutions in France or abroad, or from public or private research centers.

L'archive ouverte pluridisciplinaire **HAL**, est destinée au dépôt et à la diffusion de documents scientifiques de niveau recherche, publiés ou non, émanant des établissements d'enseignement et de recherche français ou étrangers, des laboratoires publics ou privés.



Distributed under a Creative Commons Attribution - NonCommercial - NoDerivatives 4.0 International License



## Supercritical millifluidic reactor for the synthesis of efficient GaN nanophotocatalysts

Prasaanth Ravi Anusuyadevi<sup>a</sup>, Zachary S. Campbell<sup>b</sup>, Arnaud Erriguible<sup>a</sup>, Samuel Marre<sup>a,\*</sup>, Cyril Aymonier<sup>a,\*</sup>

<sup>a</sup> Univ. Bordeaux, CNRS, Bordeaux INP, UMR5026, F-33600, France

<sup>b</sup> School of Chemical and Biomolecular Engineering, Georgia Institute of Technology, 311 Ferst Dr NW, Atlanta, GA, 30332 United States of America

### ARTICLE INFO

#### Keywords:

Continuous flow synthesis  
Chemical engineering for reactor design  
Supercritical fluids  
Gallium nitride  
Quantum dots  
Nanophotocatalysts  
Numerical modeling

### ABSTRACT

Here, we demonstrate the continuous synthesis of gallium nitride (GaN) nanophotocatalysts exhibiting high quantum confinement using a preheated supercritical millireactor. The GaN quantum dots (QDs) are obtained from the direct thermolysis of a single source amido complex precursor (tris(dimethyl)amido gallium(III) dimer), in anhydrous supercritical cyclohexane. The quality of the synthesized QDs is highly dependent on the chemical pathways for the single source precursor thermolysis. Through the use of numerical modeling, we designed a millifluidic reactor allowing a sufficiently high heating rate for a direct precursor thermolysis towards efficient GaN nanoparticles. The as-designed preheated supercritical flow reactor yields highly reproducible GaN QDs (optical properties, crystallite phase and morphology) at high throughput, enabling gram scale production. Eventually, the photocatalytic properties of the GaN QDs were evaluated in a direct photochemical reaction through the degradation of a dye molecule (Methyl Orange). The obtained results demonstrate the higher photocatalytic activity of such photocatalysts compared to the commercially and reference available Degussa P25.

### 1. Introduction

Gallium nitride (GaN) is a third generation III-V semiconducting material that exhibits several useful properties, including rigidity, mechanical stability, high chemical inertness (both in acidic and basic environments), and prolonged firmness at elevated temperatures due to high heat capacity and thermal conductivity features [1]. Furthermore, GaN also displays high breakdown electric field, high electron saturation velocity, and exceptional electron transport properties [2,3]. These attributes have recently compelled material scientists to develop various synthetic methodologies for attaining nanosized GaN particles with enhanced properties compared to bulk GaN. The large bandgap of GaN has initially driven its applications in light emitting diodes [4] but it has recently also been utilized in gas & liquid sensors [2,5–9], where GaN nanoparticles have demonstrated excellent sensing properties for gases and vapor [10,11]. Due to several redox potentials within the energy gap, GaN is now implemented in the field of heterogeneous nanophotocatalysis [12]. Unlike titanium dioxide (TiO<sub>2</sub>), GaN has only attracted interest for photocatalytic applications in the last decade.

Heterogeneous photocatalysis has been applied to numerous chemical reactions and molecular transformations, especially as a 'state of art' advanced oxidation technology (AOT) for refining water and gas effluent streams in various processes [13], and particularly the treatment of non-biodegradable textile dyes. These compounds are discharged into ground water by the dyeing industry and are responsible for 17–20% of global water pollution [14]. Indeed, compared to the traditional physical and chemical dye removal techniques, effluent remediation through heterogeneous photocatalysis is advantageous due to the low energy input, either through artificial irradiation or by direct sunlight, as well as the ease of operation and facile degradation of toxic compounds. GaN nanostructures have demonstrated attractive efficiency to degrade dyes through photoreduction processes. For instance, GaN nanowires (20 – 50 nm) synthesized by organic chemical vapor deposition have demonstrated enhanced photocatalytic activity for Orange II dye degradation under UV irradiation when compared to GaN thin films and submicron dot arrays [15]. Similarly, Fe-doped GaN nanoparticles synthesized by solid state reaction exhibit very high activity for rhodamine dye degradation under UV light [16]. In addition to

\* Corresponding authors.

E-mail addresses: [samuel.marre@icmcb.cnrs.fr](mailto:samuel.marre@icmcb.cnrs.fr) (S. Marre), [cyril.aymonier@icmcb.cnrs.fr](mailto:cyril.aymonier@icmcb.cnrs.fr) (C. Aymonier).

dye degradation, GaN nanowires have also been used to perform water splitting reactions under visible light, which is of primary interest in the development of energy efficient process for hydrogen generation [17].

To date, the synthesis of nanosized GaN photocatalysts has primarily been conducted in autoclave batch reactors at high temperatures (>800 °C) and long reaction times (10 min – 24 h) using ammonothermal methods [18] or nitration of gallium oxide nanoparticles in ammonia flows [19,20]. Recent examples also consider synthesis in ionic liquids starting from mixture of gallium and amine salts [21]. While double source precursor syntheses can provide flexibility for varying composition, they can also induce loss in reproducibility since batch mode synthesis can suffer from irreproducibility from batch to batch due to inherent gradients that can be generated inside the reactor (temperature, concentration, etc.).

To overcome these limitations, the synthesis of GaN nanomaterials has been explored using single source precursors, including gallium monoamides, diamides, and triamides. In particular, the homoleptic amido complex of gallium triamide, tris(dimethyl)amido gallium(III) dimer  $\text{Ga}_2[\text{N}(\text{CH}_3)_3]_6$  (TDAG), is among the most commonly used single source precursors for the facile synthesis of GaN nanomaterials. Two primary chemical pathways have been considered: (i) a gallium imide route in which GaN NCs are obtained from the high temperature decomposition ( $T > 500$  °C) of an intermediate polymeric gallium imide  $[\text{Ga}(\text{NH})_{3/2}]_n$  component, which can itself be formed from the reduction of TDAG at medium temperatures ( $T < 200$  °C) of TDAH [22,23] and (ii) a direct thermolysis route into which TDAG is directly decomposed at higher temperatures ( $T > 330$  °C) to GaN NCs [24]. So far, syntheses utilizing TDAG have generally been carried out in batch with long reaction times ( $16 \text{ h} < t < 24 \text{ h}$ ) under solvothermal conditions, offering poor control over the reaction parameters (heating rates, temperature gradient, concentration gradients, etc.), which leads to polydisperse nanomaterials with limited reproducibility [22–25].

To address this limitation, the transfer of GaN NCs solvothermal synthesis approaches to flow synthesis should be considered [26] as flow syntheses offer several advantages compared to their batch counterparts [27]. Indeed, continuous flow synthesis in milli-/microfluidics offers enhanced heat and mass transfer, thus shortening the synthesis time, as well as highly efficient mixing of reactive compounds, high reactivity, and maximized yield [28]. Additionally, advanced flow control of the operating parameters enables reduction of the nanomaterial polydispersity compared to batch reactors [29], while flow permits a variety of facile scaling options for further larger scale production of high quality NCs [30,31].

Furthermore, the ability to operate under a variety of pressures dramatically extends the range of solvents that can be considered for the synthesis, as they may be kept “dense” (i.e. liquid or supercritical) during the full process from room temperature to the reaction temperature. In particular, syntheses performed in supercritical fluids (SCFs), which possess high diffusivity, low viscosity, and intermediate densities, favor nucleation over growth for accessing small particle sizes by performing liquid chemistries in media that behave like gases [32]. Besides, their physical characteristics (low viscosities and high diffusivity) can narrow residence time distributions (RTD) in continuous flow reactors [33], thus enabling the synthesis of monodisperse nanoparticles [30, 34–36]. Based on such approaches, our research group has already demonstrated the continuous supercritical synthesis of GaN QDs in a tubular milli-/microreactor with coflow geometry *via* thermolysis of TDAG in supercritical cyclohexane and a hexane-ammonia mixture [26]. However, in this configuration, it was found that the reactor lifetime was limited due to clogging problems. Indeed, the injected TDAG tends to form the polymeric gallium imide intermediate ( $[\text{Ga}(\text{NH})_{3/2}]_n$ ) inside the reactor, resulting in its deposition on the reactor walls and eventually leading to clogging after several syntheses, despite the high quality of the obtained GaN NCs. The primary reason identified for this behavior was the “slow” heating rate (few tens of seconds) resulting in a two-step chemical pathway, rather than a direct thermolysis of the

precursor. Hence, one of the key parameters for accessing direct thermolysis is the control of the thermal behavior of the reactor. Mastering this parameter makes it possible to synthesize high quality GaN quantum dots, while ensuring extended operating time of the reactor, thus providing clues for scaling up the synthesis.

In this work, we investigate - using a combination of numerical and experimental studies - the thermal configuration of the coflow reactor geometry, followed by consideration of another reactor design with an incorporated preheater to achieve ultrafast temperature increase, corresponding to the optimal heating rate which enables direct thermolysis of TDAG. Instead of a two-step chemical pathway involving gallium imide polymeric intermediate formation, this configuration leads to high quality GaN QDs without reactor plugging. The synthesized GaN NCs are characterized by transmission electron microscopy (TEM), X-ray diffraction (XRD), X-ray photoelectron spectroscopy (XPS), and UV-Vis absorbance. Finally, their photochemical efficiency is compared to Degussa P25  $\text{TiO}_2$  NPs for the photocatalytic degradation of Methyl Orange (MO), showing a degradation rate of MO 5.2 times higher than the reference  $\text{TiO}_2$ .

## 2. Experimental section

### 2.1. Micro-millifluidic reactors

Two continuous reactor configurations were considered. They both share the same main reactor section, which was made up of a three-meter long, 1/16" (1 mm ID) stainless steel tube. The reactors were fabricated by manually coiling the tubing around a heating cartridge (Acim Jouanin, 800 W, 230 V), whose temperature is controlled by a temperature controller (Eurotherm®). The total volume of the reactor corresponds to 2.36 mL. At the outlet of the reactor, the reaction medium temperature is quenched by using a coiled tube immersed in an ice bath. A backpressure regulator (BPR) (Jasco BP-4380) is placed at the outlet of the reactor to control and maintain a constant pressure inside the reactor. The outlet of the BPR is connected to the collection bottle made up of borosilicate material to collect the synthesized GaN QDs. The precursor solution and solvent are injected using JASCO (HPLC) high-pressure pumps (model PU-4180), while the solvent is stored in specially designed solvent tank with tight rubber seals and a four-valve system for solvent suction and argon gas injection. The remaining valves act as vents for the solvent tank so that continuous flow of argon gas is maintained.

The difference between the two reactor configurations primarily involves the fluid mixing strategy before entering the reactor. The coflow reactor (Fig. 1A) is composed of a 1/32" SS capillary (ID: 400  $\mu\text{m}$ ) inserted inside a 1/16" SS tubing (ID: 1 mm), thus forming a concentric tubing arrangement, as previously reported [31,37]. The precursor at room temperature is injected as the inner flow, while the outer flow is only composed of pure cyclohexane at room temperature, which helps generate a jet to confine the nucleation of the NCs far from the reactor wall. The length of the inner tubing is fixed so that the jet is generated exactly at the inlet section of the main reactor. In the second configuration (Fig. 1B) a preheated line is added to the set-up so that the pure cyclohexane solvent is heated to 400 °C and mixed with the RT precursor flow in a T-shaped mixer, thus creating a hot mixing zone. The resultant hot fluid enters the reactor, where the walls are maintained at 400 °C. The preheater is made of a one-meter long 1/32" (400  $\mu\text{m}$  ID) SS tube coiled around a heating cartridge, similar to the main reactor.

### 2.2. Synthesis of GaN QDs

Tris(dimethylamido)-gallium(III), 99.9% (metal basis) from Alfa-Aesar and cyclohexane (anhydrous, 99.5%) from Sigma-Aldrich were purchased and used without further purification or processing in the synthesis methodology. Solvent and precursors were received in inert gas-filled packing and were stored in a glove box to prevent water or

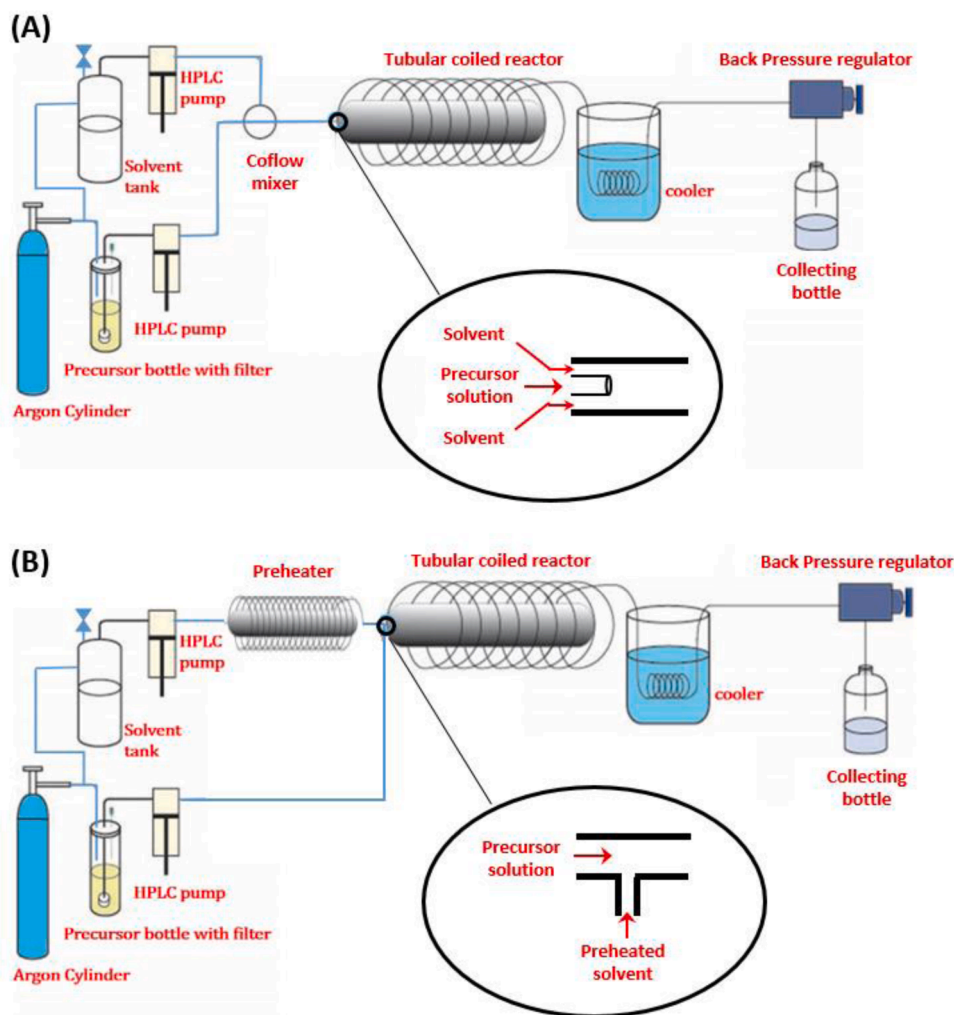


Fig. 1. (A) Coflow reactor and (B) preheater reactor used for the production of GaN QDs at supercritical conditions (400 °C, 150 bar).

oxygen contamination. In a typical synthesis, the precursor solution (concentration 0.035 M) was prepared inside the glove box by adding 500 mg of precursor to 35 mL of anhydrous cyclohexane in a specially designed precursor bottle. Two high-pressure pumps were used to deliver the precursor solution and pure solvent, respectively, to the reactor. In both reactor configurations, the temperature of the reactor wall was fixed at 400 °C and the overall pressure was 150 bar, well above the critical conditions of cyclohexane (281 °C, 40.7 bar). The precursor and preheated cyclohexane streams were each injected into the reactor at a rate of 1 mL/min, creating a precursor concentration of 0.017 M inside the millireactor for an overall residence time of  $\approx 30$  s.

For the coflow configuration, the precursor was injected as the inner flow, while pure cyclohexane was injected coaxially, before entering the reactor. For the preheater reactor configuration, the precursor solution (at RT) was co-injected with the preheated cyclohexane (400 °C) inside a T-junction before entering the reactor. The resulting colloidal suspension of GaN NCs was collected downstream the BPR and analysed. The suspensions were first centrifuged at 10,000 rpm for 15 min, the supernatant removed, redispersed in ethanol, and drop cast onto a copper carbon grid for TEM characterization. For XPS characterization, the samples were first centrifuged at 10,000 rpm for 15 min and the collected powder was dried in an oven overnight at 80 °C before being deposited on carbon tape.

### 2.3. Photocatalytic testing of GaN QDs

To test the photocatalytic activity of the synthesized GaN QDs and compare them with the one of conventional Degussa P25 TiO<sub>2</sub> nanoparticles, we considered a triphasic system including nanophotocatalysts, a DI water phase, and an atmospheric air phase, used as the gas source in this study. A suspended (slurry) photoreactor was fabricated and employed in this study (see ESI-1). It consists of a cylindrical glass tube fitted with a rubber septum. The suspension of photocatalyst within the photoreactor is achieved by magnetic stirring. The tube was placed in an illumination chamber consisting of a hollow cylindrical (outer) vessel. The inner surface of the vessel is coated with a highly reflective aluminum tape, while LED strips (24 W, 3.5 m long, 200 LEDs,  $\lambda_{\max} = 400$  nm – see Fig. S1 in ESI-1) are used as light sources. This way, the cylindrical reactor is exposed to an equal quantity of photons in all directions with a radial illumination. At the bottom of the photocatalytic setup, an airline (air flow @ 4–6 bar pressure) was used to maintain constant room temperature conditions.

In a typical experiment, 5 mL of distilled water was added to a certain amount of dye (Methyl Orange - MO) to reach a concentration of  $8.3 \cdot 10^{-5}$  M. Then, 3 mg of photocatalyst was added to the vessel, which was stirred and closed at the top with a septum. The system was slightly pressurized by installing an air balloon at the top of the reactor via a syringe needle. The system was first stirred for 10 min in the dark so that adsorption-desorption equilibrium of the reactive molecules on the nanophotocatalysts surface was attained before LEDs were switched on.

The dye degradation was monitored by UV–Vis absorption spectroscopy at  $\lambda_{\text{max}} = 464 \text{ nm}$ .

### 3. Results and discussions

#### 3.1. Numerical simulation: thermal behavior of the reactors

Heat transfer modeling studies were performed for the two reactor designs to evaluate the effect of the mixing point strategy over the thermal behavior. Indeed, as mentioned previously, reactor operation temperatures below  $330 \text{ }^\circ\text{C}$  result in polymerization of the precursor and reactor fouling, while temperatures above  $330 \text{ }^\circ\text{C}$  enable direct thermolysis of the single source GaN precursor to GaN NCs. In this numerical modeling study, the cyclohexane stream was considered monophasic, compressible, and non-isothermal. Indeed, in such synthetic process, the reactive medium undergoes transcritical phase change from a dense incompressible liquid phase to a supercritical compressible phase, thus resulting in huge density changes inducing an increase in fluid velocities. This phenomenon is primarily due to the constant mass flow rate imposed by the high-pressure pumps. Hence, to compensate for density change, the fluid increases its speed when undergoing loss in density, which affects the overall fluid properties, including heat capacity and thermal diffusivity, that must be taken into account in the numerical modeling.

To do so, the Navier-Stokes equation and the energy conservation equation are solved for a compressible single-phase flow formulation specially developed to capture the high variability of thermophysical properties for transcritical flows [38,39]. The thermophysical properties are calculated using the NIST library. The partial differential system is solved numerically by the in-house Fortran CFD code "Notus" (<https://notus-cfd.org/>), developed at the Institute of Mechanical Engineering (I2M-TREFLE). Notus is an open source software based on the finite volume method. The variable fields are solved on a fixed staggered grid. As Notus is massively parallel, it allows high accuracy simulation [40]. The formulation used is fully implicit and second order schemes are preferred for temporal and spatial discretizations. All details can be found in our previous articles.

Fig. 2A presents the thermal profile inside the coflow reactor, while the average temperature of the fluid at the center of the tubing reactor is plotted as a function of time (Fig. 2C) and distance from the mixing point (Fig. 2D). As seen, it takes approximately 1 s to reach only a temperature of  $200 \text{ }^\circ\text{C}$  (Fig. 2C). This "slow" temperature increase in the coflow reactor geometry generates an intermediate temperature zone ( $100 - 300 \text{ }^\circ\text{C}$ ) of roughly few tens of centimeters in the reactor (Fig. 2D), in which the TDAG precursor can react to form the non-soluble intermediate polymeric gallium imide  $[\text{Ga}(\text{NH})_{3/2}]_n$  component, resulting in precipitation, which limits reactor throughput and lifetime.

By comparison, it was observed that a temperature increase is achieved rapidly with the preheater reactor configuration (Fig. 2B and movie M1 in ESI). As seen, the preheated cyclohexane solvent ( $400 \text{ }^\circ\text{C}$ ) is mixed with the RT precursor solution and the resulting mixture reaches  $\approx 330 \text{ }^\circ\text{C}$  in less than  $0.05 \text{ s}$  (Fig. 2C), i.e. less than 1 cm after the mixing area (Fig. 2D). With this new thermal configuration, a direct thermolysis of the single TDAG precursor is performed, resulting in high reproducibility along with a substantial increase of the reactor lifetime (no clogging was observed after 50 runs of continuous individual synthesis), allowing for producing  $\approx 2-3 \text{ g}$  per day of high quality GaN QDs.

Therefore, while coflow strategies could prevent heterogeneous nucleation on the reactor walls (by flow focusing the nucleation step) and have been demonstrated to be excellent for continuous synthesis of

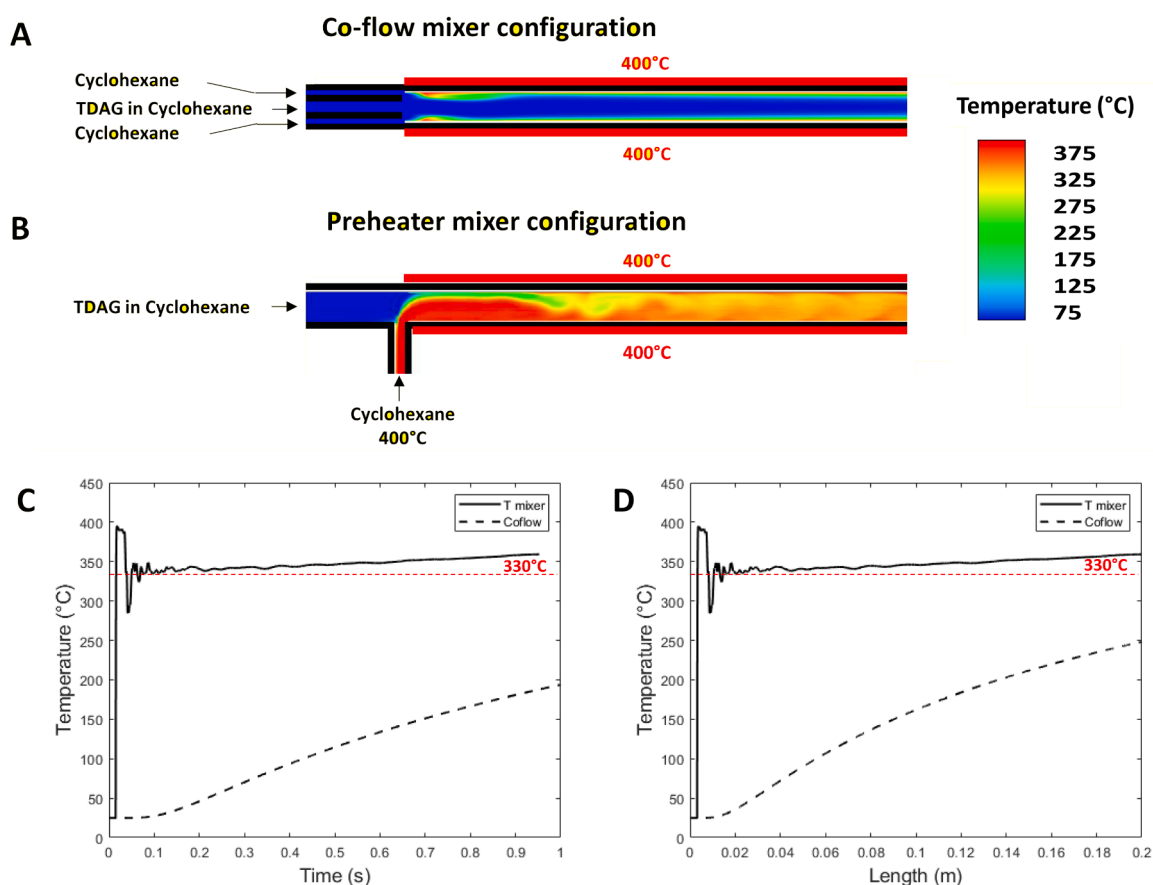


Fig. 2. Thermal profile in the coflow reactor (A) and in the reactor fed with preheated cyclohexane (B). (C) Temperature of the reactive fluid at the center of the tubing reactor as a function of time (C) and distance from the mixing point (D) obtained through direct numerical simulation.

several NC types [35,37], it appears that when chemical intermediates can be generated during the chemical pathway within a particular temperature range, this low Reynolds number (*i.e.* laminar) strategy is not ideal. For GaN NCs synthesis from single source TDAG, which appears to be the most promising from a chemical point of view, the heating rate is clearly the limiting step for performing continuous flow synthesis. Therefore, ultra-fast mixing of the precursor solution with a preheated solution appears to be the best solution to quickly attain the direct thermolysis temperature, preventing intermediate formation and deposition onto the reactor walls.

### 3.2. Materials characterization

Powder X-Ray diffraction was performed using a silicon substrate with zero background. The diffraction spectrum shows that GaN nanomaterials display a wider peak, similar to patterns already reported for nanosized GaN [23,41,42]. Comparison of the obtained diffraction pattern with JCPDS cards shows that the synthesized GaN nanomaterials contain both hexagonal and cubic phases. The XRD pattern presents a uniform wider peak with maximum intensity at 35° corresponding to the (111) lattice plane of Zinc blende GaN, while a shoulder is observed in the 40–50° region, emerging from the NaCl-Cubic phases present in the sample (Fig. 3).

Characterization of particle size, morphology, and crystallite phase was performed using high resolution transmission electron microscopy (HRTEM). Large spherical aggregates (50–100 nm) (Fig. 4A) composed of nanoparticles with size averaging  $2.8 \pm 0.6$  nm in diameter are mostly present, while small dispersed nanoparticles were also distinguishable in a much lower proportion, which were used for size measurements (see ESI-2). The average nanoparticle size falls below the Bohr exciton radius of bulk GaN (2.8 nm)[43], thus indicating that quantum confined nanocrystals were synthesized.

HRTEM was then used to investigate the crystalline phases present in the synthesized GaN NCs using a D-spacing measurement. The identified D-spacing values depend on the lattice fringes observed in the NP samples. Both GaN hexagonal wurtzite ((100) and (101) lattice planes) and Rocksalt cubic structures ((200) lattice plane) were identified in different regions of same spherical aggregate sample (Fig. 4B and C).

The GaN QDs surface properties were then characterized by XPS. The XPS survey showed the presence of Ga, O, and C chemical elements. Fig. 5A shows that the Ga2p<sub>3</sub> maximum peak occurs at 1117.9 eV, which indicates some Ga<sub>2</sub>O<sub>3</sub> bonding. As the N1s peak overlapped with the GaLM1 Auger line (Fig. 6B), no conclusion concerning the presence of N can be obtained. The presence of carbon and oxygen may be attributed to contamination due to atmospheric exposure and the use of organic solvents for washing, centrifugation, and dispersion.

To reveal the subsurface nature of the synthesized GaN NCs, depth profiling was carried out to etch the contaminated top layers. Etching was performed using argon ion gun sputtering at low energy at a rate of

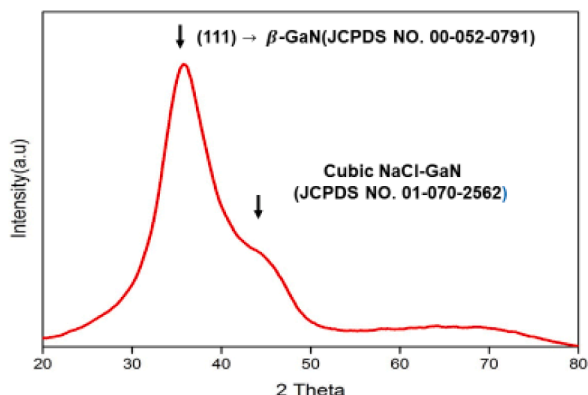


Fig. 3. X-Ray diffraction pattern of the synthesized GaN nanoparticles.

approximately 0.2 nm/s. At each interval of 30 s, the etching was stopped and high resolution Ga2p<sub>3</sub> and N1s photoelectron spectra were recorded. In the Ga2p<sub>3</sub> sputtered spectrum (Fig. 6A), the appearance of a low energy component at 1116.4 eV confirms the presence of Ga-N bonding consistent with previously reported XPS spectra of GaN samples [44–46].

Fig. 6B presents XPS spectra of the N1s-GaLM1 range. Interestingly, it was observed that the main peak shifted from 397.8 eV to 397.1 eV with increasing depth indicates the presence of subsurface N1s nitride bonding. Furthermore, a smaller peak around 392 eV is characteristic of the GaLM1 Auger line in the nitride form, meaning that GaN QDs with many unsatisfied dangling bonds were synthesized. These unpassivated surface states act as bonding sites for contaminants, especially oxygen, during post processing.

Similar results were obtained for the GaN QDs synthesized with the coaxial reactor, demonstrating that the chemical pathway has no effect on the final structure and size of the particles (see ESI-3).

### 3.3. Characterization of the optical properties

Following chemical and microscopic characterization, the dispersed nanoparticles were characterized optically via UV-Vis absorption. The synthesized GaN NCs were first centrifuged at 10,000 rpm and redispersed in acetonitrile. The colloidal suspensions were found to exhibit a maximum peak at 302 nm (Fig. 7).

The characteristic absorption band edge was blue shifted by 85 nm compared to bulk cubic zinc blende (387 nm) and 58 nm compared to hexagonal wurtzite GaN (365 nm) indicating that highly quantum confined GaN QDs were obtained from the continuous supercritical synthesis. The optical direct energy gap was calculated from the relationship between the absorption coefficient of the material and incident photon energy as seen in Eq. (1):

$$\alpha \cdot hv = A \cdot (hv - E_{\text{sample}})^n \quad (1)$$

where  $E_{\text{sample}}$ ,  $A$ , and  $hv$  correspond to the energy gap of the sample measured, a constant, and energy of the incident photon, respectively. The absorption coefficient,  $\alpha$ , was determined from Beer Lambert's law (Eq. (2)):

$$\alpha = (2.303 \cdot \text{Absorbance}) / l \quad (2)$$

where  $l$  refers to the path length of the liquid cell used in the absorption measurement ( $l = 1$  cm).

The inset graph in Fig. 7 presents a plot of  $(\alpha hv)^2$  [2] as a function of  $hv$  (eV) for the GaN QDs (Tauc plot). The optical band gap energy was obtained by the linear extrapolation of the Tauc curve at  $y = 0$ , or  $(\alpha hv)^2 \rightarrow 0$ . The optical band gap obtained from the Tauc plot was 3.8 eV. The obtained value indicates that highly quantum confined GaN nanoparticles were synthesized, with blue shifts of 0.6 eV and 0.4 eV compared to cubic zinc blende (3.2 eV) and hexagonal wurtzite GaN (3.4 eV), respectively [47]. The band gap shift is attributable to the size-dependent quantization effect, where the relationship between the band gap shift,  $\Delta E = E_{\text{QD}} - E_{\text{bulk}}$ , and the quantum dot size can be related using the Brus effective mass model [48–51]. The radius of the spherical GaN QDs can be determined using the relationship seen in Eq. (3) [47]:

$$\Delta E = \frac{h^2}{8\mu R^2} - \frac{1.786e^2}{4\pi\epsilon_{\text{QD}}\epsilon_0 R} \quad (3)$$

where  $\Delta E = 0.96 \cdot 10^{-19}$  J,  $h$  is the Planck's constant,  $R$  is the estimated QD radius,  $e$  is the charge of an electron, and  $\epsilon_0$  is the vacuum dielectric constant.

The size dependent static dielectric constant expression (Eq. (4)) was used, as  $\epsilon_{\text{QD}}$  varies significantly for the GaN QDs, particularly compared to three-dimensional bulk GaN.

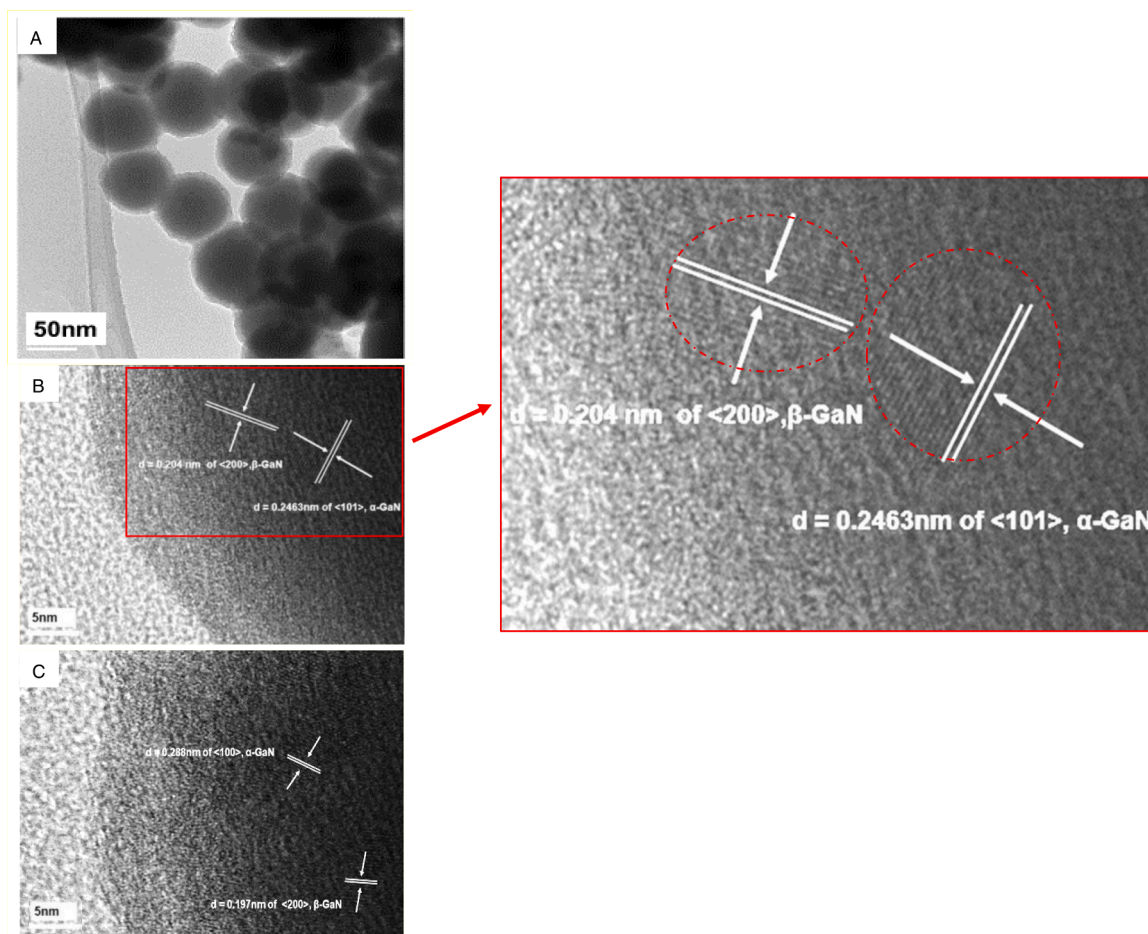


**Fig. 4.** A) Spherical aggregates of GaN QDs. B) Wurtzite ( $\beta$ -GaN) and cubic ( $\alpha$ -GaN) coherent domains observed with HRTEM in different regions of the spherical aggregates, along with a zoom for better visualization of the lattice fringes. C) Co-existence of different monocrystalline structures within a spherical aggregate.

$$\epsilon_{\text{QD}} = 1 + \frac{\epsilon_{3\text{D}} - 1}{1 + \left[ \frac{\Delta E^2}{E_{\text{QD}}^2} \right]} \quad (4)$$

In this expression,  $\Delta E$  was 0.6 eV for zinc blende GaN and 0.4 eV for wurtzite,  $E_{\text{QD}} = 3.8$  eV, and  $\epsilon_{3\text{D}}$  was 9.7 eV for zinc blende or 8.9 eV for wurtzite. Both zinc blende and wurtzite crystallite structures were considered, as powder XRD and HRTEM both confirmed that the synthesized QDs possessed both zinc blende and wurtzite monocrystallites. The calculated  $\epsilon_{\text{QD}}$  was found to be 9.488 eV and 8.813 eV for zinc blende and wurtzite, respectively. Similarly,  $\mu$  was also calculated for zinc blende and wurtzite from effective electrons and holes mass using  $m_0$ , which refers to electron rest mass ( $9.1095 \times 10^{-31}$  kg). Substituting these values and solving Eq. (3) yields to QD radii of 14.0 Å and 19.8 Å for zinc blende and wurtzite structures, respectively. The values obtained here fall below the Bohr exciton radius of bulk GaN (27 Å) [52], further suggesting that quantum confined nanoparticles were synthesized.

We found similar optical properties for the GaN QDs synthesized with the coaxial reactor (see ESI-4).

### 3.4. Evaluation of the photocatalytic efficiency

The synthesized GaN QDs were then compared with commercially available Degussa P25 TiO<sub>2</sub> for the direct photodegradation of methyl orange (MO). The spherical GaN QD aggregates used were polycrystalline, possessing both zinc blende and wurtzite phases. By comparison, the commercial Degussa P25 is a mixture of crystalline TiO<sub>2</sub> anatase and rutile, with approximately 70–80% anatase, 10–20% rutile,

and the remainder amorphous [53]. The average crystal size is 85 nm for anatase and 25 nm for rutile [54]. Anatase possesses a band gap of 3.2 eV (385 nm) [55], while the band edge of rutile extends up to 3.0 eV (410 nm) [56].

For this photocatalytic study, direct dye photodegradation was performed using a low power LED light source (395–405 nm) with a maximum intensity at 400 nm. During illumination, the dye molecule methyl orange (MO), which possesses a maximum absorption edge at 464 nm, was excited. Upon excitation, MO transfers the excited electron to the ground state semiconductor, which then reacts with surface-bound oxygen, forming superoxide radicals. The formed superoxide radicals then react with the solvent, resulting in hydroxyl radicals, which then degrade the azo bonds present in the dye [57]. These reactions were studied through the reduction in absorbance at 464 nm (dye absorbance) over the course of 3 h (Fig. 8A). A 100% dye photodegradation of the azo bond when using the produced GaN photocatalysts occurred within 3 h, as indicated by the complete disappearance of the peak at 464 nm. The photodegradation experiment was then repeated using the Degussa P25 photocatalyst. It was observed that in 3 h, only 50% of the dye was degraded using TiO<sub>2</sub> (Fig. 8B).

The higher photocatalytic activity observed for the GaN photocatalyst may be attributed to difference in the average NP size, as it directly impacts surface area and availability of catalytic active sites. The low average GaN QD particle sizes, 2.80 nm for cubic zinc blende and 3.96 nm for wurtzite, compared to 85 nm anatase and 25 nm rutile crystals strongly suggests that the synthesized GaN QDs possess higher specific surface areas than commercially available Degussa P25. Besides, the synthesized GaN QDs possess large quantities of unsatisfied atomic

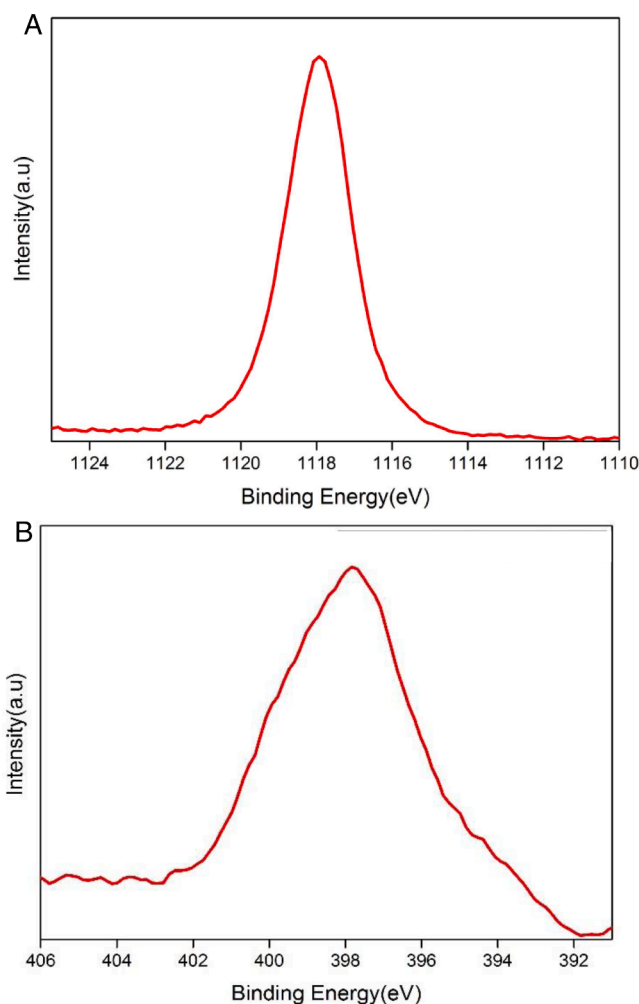


Fig. 5. A) Ga<sub>2p<sub>3</sub></sub> spectra of the GaN NCs surface. B) N1s spectra of the GaN NCs surface.

orbitals on their surfaces, which could act as bonding sites for oxygen molecules during the photocatalysis. The presence of these bonding sites was confirmed through XPS analysis, where oxygen was observed bonding to these GaN QD surface sites. Furthermore, the distinctive GaN QDs agglomeration also accelerates electron transport (possibly through the antenna effect) from the excited dye to the oxygen molecule enabling a photodegradation rate 5.2 times higher than Degussa P25.

#### 4. Conclusion

In heterogeneous photocatalysis, one of the primary limitation to date concern the development of fast, efficient and reliable processes to synthesize advanced nanophotocatalysts. The particular case of GaN quantum dots was investigated in this study. Here, we have reported the rapid, facile synthesis of quantum confined GaN QDs through a pre-heated supercritical millireactor. Numerical modeling of the thermal behavior in the reactor demonstrated that such a design allows a direct pyrolysis of the single-source tris(dimethyl)amido gallium(III) (TDAG) to GaN QDs, avoiding the formation of an intermediate polymeric gallium imide  $[\text{Ga}(\text{NH})_3/2]_n$  component. This development enables synthesis at high throughputs (up to gram scale per day), while improving the reactor lifetime by fixing the issue of clogging due to intermediate deposition on the reactor walls. The synthesized GaN QDs were observed to be well dispersed large spherical agglomerates (50–100 nm) composed of small GaN QDs ( $2.8 \pm 0.6$  nm) crystallized in cubic zinc blende or hexagonal wurtzite phases (XRD and HRTEM). The presence

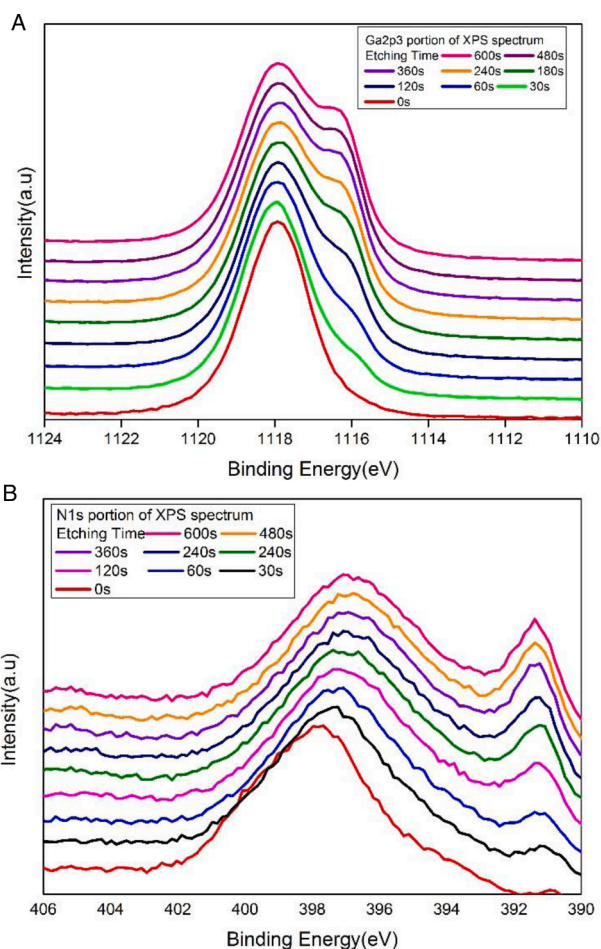


Fig. 6. A) Ga<sub>2p<sub>3</sub></sub> sputtered portion of XPS spectrum of GaN, total etching time 600 s with a sputtering rate of 0.2 nm/s, spectra recorded every 30 s. B) N1s sputtered portion of XPS spectrum of GaN, total etching time 600 s with sputtering rate of 0.2 nm/s, spectra recorded every 30 s.

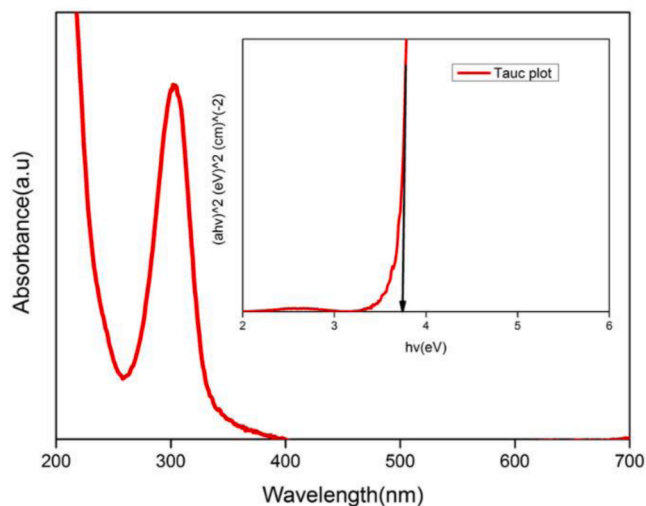
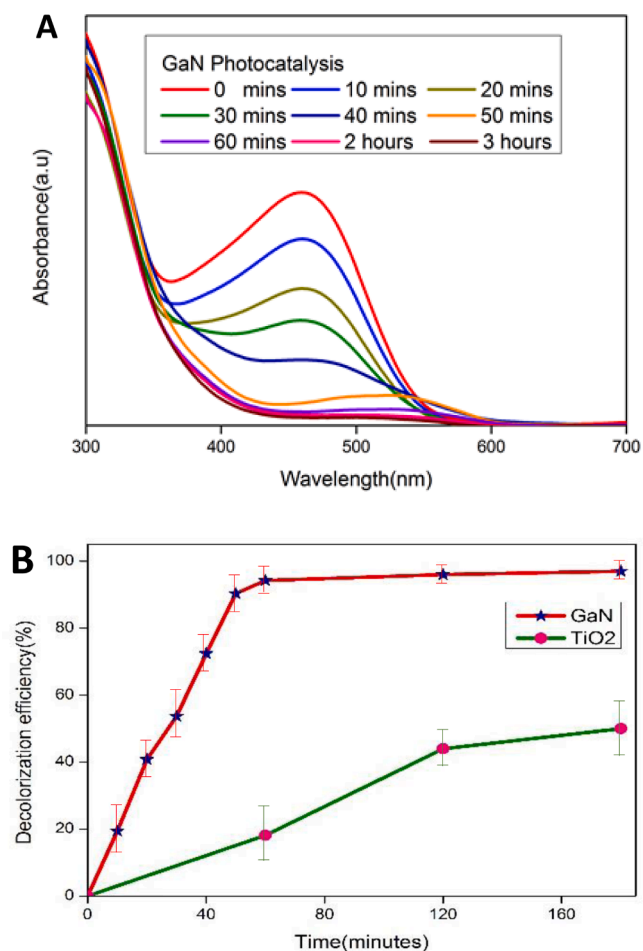


Fig. 7. Absorption spectrum of the GaN QDs dispersed in acetonitrile. Inset: Tauc plot of the presented absorption.

of Ga-N bonding, along with slight surface oxygen contamination, was confirmed through XPS. The optical properties of the as synthesized GaN QDs were determined and their photocatalytic efficiency was tested



**Fig. 8.** A) UV-VIS absorption spectra of GaN photocatalyzed MO solution at different time intervals. B) Comparison of the dye photodegradation by GaN and TiO<sub>2</sub> over 3 h.

against commercial Degussa P25 TiO<sub>2</sub> for the direct photodegradation of methyl orange (MO). It was found that GaN QDs can degrade MO 5.2 times faster than TiO<sub>2</sub>. The improvement of the reactor design therefore opens avenues towards fast, efficient and scalable continuous processes (up to 1 g/day of GaN QDs in this study) for high quality photocatalytic nanomaterials.

#### Funding information

This work has received funding from the European Union's Horizon 2020 research and innovation program under the Marie Skłodowska-Curie grant agreement No 641861: Photo4Future project.

#### Declaration of Competing Interest

The authors declare the following financial interests/personal relationships which may be considered as potential competing interests: Samuel MARRE reports financial support was provided by European Union.

#### Data availability

Data will be made available on request.

#### Supplementary materials

Supplementary material associated with this article can be found, in the online version, at doi:10.1016/j.cej.2023.100483.

#### References

- [1] N.M. Ghazali, K. Yasui, A.M. Hashim, *Nanoscale Res. Lett.* 9 (2014) 1–8.
- [2] D.-S. Lee, J.-H. Lee, Y.-H. Lee, D.-D. Lee, *Sens. Actuators B: Chem.* 89 (2003) 305–310.
- [3] M. Mohamad, F. Mustafa, M.S.Z. Abidin, S.F. Abd Rahman, N.K.A. Al-Obaidi, A.M. Hashim, A.A. Aziz and M.R. Hashim, 2010 IEEE International Conference on Semiconductor Electronics (ICSE2010), Malacca, Malaysia, 2010, pp. 301–304.
- [4] H. Jia, L. Guo, W. Wang, H. Chen, *Adv. Mater.* 21 (2009) 4641–4646.
- [5] J. Schallwig, G. Müller, O. Ambacher, M. Stutzmann, *Phys. Status Solidi* 185 (2001) 39–45.
- [6] B.H. Chu, B.S. Kang, S.C. Hung, K.H. Chen, F. Ren, A. Sciuillo, B.P. Gila, S. Pearton, *J. Diabetes Sci.* 4 (2010) 171–179.
- [7] S.J. Pearton, F. Ren, *IEEE Instrum. Meas. Mag.* 15 (2012) 16–21.
- [8] M.S.Z. Abidin, A.M. Hashim, M.E. Sharifabad, S.F.A. Rahman, T. Sadoh, *Sensors* 11 (2011) 3067–3077.
- [9] M.S.Z. Abidin, H.A. Shahjahan, A.M. Hashim, *Sains Malays.* 2 (2013) 197–203.
- [10] N.M. Ghazali, M.R. Mahmood, K. Yasui, A.M. Hashim, *Nanoscale Res. Lett.* 9 (2014) 1–7.
- [11] B. Chitara, D.J. Late, S. Krupanidhi, C. Rao, *Solid State Commun.* 150 (2010) 2053–2056.
- [12] C. Xu, P.R. Anusuyadevi, C. Aymonier, R. Luque, S. Marre, *Chem. Soc. Rev.* 48 (2019) 3868–3902.
- [13] J.-M. Herrmann, *Catal. Today* 53 (1999) 115–129.
- [14] A. Ajmal, I. Majeed, R.N. Malik, H. Idriss, M.A. Nadeem, *RSC Adv.* 4 (2014) 37003–37026.
- [15] H.S. Jung, Y.J. Hong, Y. Li, J. Cho, Y.-J. Kim, G.-C. Yi, *ACS Nano* 2 (2008) 637–642.
- [16] H. Tong, J. Wang, M. Wang, B. Chen, Q. Shi, J. Ma, *Superlattices Microstruct.* 78 (2015) 12–21.
- [17] M. Kibria, F. Chowdhury, S. Zhao, B. AlOtaibi, M. Trudeau, H. Guo, Z. Mi, *Nat. Commun.* 6 (2015) 1–8.
- [18] W. Wang, Y. Xu, D. Zhang, X. Chen, *Mater. Res. Bull.* 36 (2001) 2155–2162.
- [19] T. Ogi, Y. Kaihatsu, F. Iskandar, E. Tanabe, K. Okuyama, *Adv. Powder Technol.* 20 (2009) 29–34.
- [20] F. Iskandar, T. Ogi, K. Okuyama, *Mater. Lett.* 60 (2006) 73–76.
- [21] H.F. Gaiser, R. Popescu, D. Gerthsen, C. Feldmann, *Chem. Commun.* 56 (2020) 2312–2315.
- [22] J.F. Janik, R.L. Wells, *Chem. Mater.* 8 (1996) 2708–2711.
- [23] O. Micić, S. Ahrenkiel, D. Bertram, A.J. Nozik, *Appl. Phys. Lett.* 75 (1999) 478–480.
- [24] G. Pan, M.E. Kordesch, P.G. Van Patten, *Chem. Mater.* 18 (2006) 3915–3917.
- [25] J.L. Coffey, M.A. Johnson, L. Zhang, R.L. Wells, J.F. Janik, *Chem. Mater.* 9 (1997) 2671–2673.
- [26] B. Giroire, S. Marre, A. Garcia, T. Cardinal, C. Aymonier, *React. Chem. Eng.* 1 (2016) 151–155.
- [27] R.L. Hartman, J.P. McMullen, K.F. Jensen, *Angew. Chem. Int. Ed.* 50 (2011) 7502–7519.
- [28] S.A. Khan, A. Günther, M.A. Schmidt, K.F. Jensen, *Langmuir* 20 (2004) 8604–8611.
- [29] S. Marre, K.F. Jensen, *Chem. Soc. Rev.* 39 (2010) 1183–1202.
- [30] A. Chakrabarty, S. Marre, R.F. Landis, V.M. Rotello, U. Maitra, A. Del Guero, C. Aymonier, *J. Mater. Chem. C* 3 (2015) 7561–7566.
- [31] E.S. Ilin, S. Marre, V. Jubera, C. Aymonier, *J. Mater. Chem. C* 1 (2013) 5058–5063.
- [32] C. Aymonier, G. Philippot, A. Erriguible, S. Marre, *J. Supercrit. Fluids* 134 (2018) 184–196.
- [33] S. Marre, Y. Roig, C. Aymonier, *J. Supercrit. Fluids* 66 (2012) 251–264.
- [34] S. Marre, J. Park, J. Rempel, J. Guan, M.G. Bawendi, K.F. Jensen, *Adv. Mater.* 20 (2008) 4830–4834.
- [35] Y. Roig, S. Marre, T. Cardinal, C. Aymonier, *Angew. Chem. Int. Ed.* 50 (2011) 12071–12074.
- [36] C. Slostowski, S. Marre, J.-M. Bassat, C. Aymonier, *J. Supercrit. Fluids* 84 (2013) 89–97.
- [37] T. Gendrineau, S. Marre, M. Vaultier, M. Pucheault, C. Aymonier, *Angew. Chem. Int. Ed.* 124 (2012) 8653–8656.
- [38] T. Voisin, A. Erriguible, G. Philippot, D. Ballenghien, D. Mateos, F. Cansell, B. B. Iversen, C. Aymonier, *Chem. Eng. Sci.* 174 (2017) 268–276.
- [39] S. Amiroudine, J.-P. Caltagirone, A. Erriguible, *Int. J. Multiph. Flow* 59 (2014) 15–23.
- [40] F. Zhang, S. Marre, A. Erriguible, *Chem. Eng. J.* 382 (2020), 122859.
- [41] G. Pan, M.E. Kordesch, P.G. Van Patten, *Chem. Mater.* 18 (2006) 5392–5394.
- [42] J.-W. Hwang, J.P. Campbell, J. Kozubowski, S.A. Hanson, J.F. Evans, W. L. Gladfelter, *Chem. Mater.* 7 (1995) 517–525.
- [43] P. Ramvall, P. Riblet, S. Nomura, Y. Aoyagi, S. Tanaka, *J. Appl. Phys.* 87 (2000) 3883–3890.
- [44] Y. Yang, V.J. Leppert, S.H. Risbud, B. Twamley, P.P. Power, H.W. Lee, *Appl. Phys. Lett.* 74 (1999) 2262–2264.
- [45] R. Carin, J. Deville, J. Werckmann, *Surf. Interface Anal.* 16 (1990) 65–69.
- [46] S. Wolter, B. Luther, D. Waltemyer, C. Önnby, S.E. Mohny, R. Molnar, *Appl. Phys. Lett.* 70 (1997) 2156–2158.

- [47] K. Dimos, L. u. Jankovič, I.B. Koutselas, M.A. Karakassides, R. Zboril, P. Komadel, *J. Phys. Chem. C* 116 (2012) 1185–1194.
- [48] L.E. Brus, *J. Chem. Phys.* 80 (1984) 4403–4409.
- [49] L. Brus, *J. Phys. Chem.* 90 (1986) 2555–2560.
- [50] Y. Kavanuma, *Phys. Rev. B* 38 (1988) 9797.
- [51] D. Denzler, M. Olschewski, K. Sattler, *J. Appl. Phys.* 84 (1998) 2841–2845.
- [52] G. Steude, T. Christmann, B. Meyer, A. Goeldner, A. Hoffmann, F. Bertram, J. Christen, H. Amano, I. Akasaki, *Mater. Res. Soc. Int. J. Nitride Semiconductor Res.* 4 (1999) 244–249.
- [53] B. Ohtani, O. Prieto-Mahaney, D. Li, R. Abe, *J. Photochem. Photobiol. A: Chem.* 216 (2010) 179–182.
- [54] T. Ohno, K. Sarukawa, K. Tokieda, M. Matsumura, *J. Catal.* 203 (2001) 82–86.
- [55] U. Stafford, K.A. Gray, P.V. Kamat, A. Varma, *Chem. Phys. Lett.* 205 (1993) 55–61.
- [56] D.C. Hurum, A.G. Agrios, K.A. Gray, T. Rajh, M.C. Thurnauer, *J. Phys. Chem. B* 107 (2003) 4545–4549.
- [57] A. Petrella, D. Spasiano, P. Cosma, V. Rizzi, M. Race, M.C. Mascolo, E. Ranieri, *Processes* 9 (2021) 205.